Catalysis Letters Vol. 100, Nos. 1–2, March 2005 (© 2005)
DOI: 10.1007/s10562-004-3086-9

Effects of channel structure and acidity of molecular sieves in hydroisomerization of *n*-octane over bi-functional catalysts

Hu Yunfeng,[a,b] Wang Xiangsheng,[a] Guo Xinwen,[a,*] Li Silue,[b] Hu Sheng,[c] Sun Haibo,[b] and Bai Liang[b]

[a]*Department of Catalysis Chemistry and Engineering, State Key Laboratory of Fine Chemicals, Dalian University of Technology, Dalian, 116012 P R China*
[b]*PetroChina Daqing Refining & Chemical Company, Daqing, 163411 P R China*
[c]*Research Institute of PetroChina Daqing Petrochemical Company, Daqing, 163714 P R China*

Received 12 August 2004; accepted 17 November 2004

SAPO-5, -11, -31, -41, -34, ZSM-5, -22 and -23 were synthesized by using the hydrothermal method and characterized by various methods such as XRD, SEM, XRF and TPD of NH_3. They are representative of large-pore, medium-pore, small-pore, weak acid, strong acid, monodimensional channel and zigzag channel type of molecular sieves. Effects of pore size, the number of acid sites over medium-pore SAPOs, acid strength and shape of medium-pore channel on hydroisomerization of *n*-octane were examined over Pt-loaded corresponding molecular sieves. These results indicate that the selectivity to isomerization in hydroisomerization of *n*-octane is highly influenced by channel structure in molecular sieves and the conversion activity of *n*-octane is dependent on acidity of molecular sieves. Monodimensional medium-pore molecular sieves are ideal catalytic materials for higher isomerization selectivity in hydroisomerization of *n*-octane regardless of acid strength, such as SAPO-11, -31, -41, ZSM-22 and -23.

KEY WORDS: Hydroisomerization; bi-functional catalyst; *n*-octane; channel; acidity; SAPO-41; SAPO-31; SAPO-11; ZSM-22; ZSM-23.

1. Introduction

Catalytic dewaxing process was first commercialized by Mobil using ZSM-5 catalyst [1] and the process is carried out by selective cracking long chain *n*-paraffins, resulting in significant yield loss during increasing the low temperature performance of the lubes. Lubes and middle-distillate fuels with advanced performance, environmental and safety benefits are in increasing demand [2]. The hydroisomerization of *n*-paraffins has made possible the production of higher quality lubes and fuels with low pour points at higher yield.

Bi-functional catalysts containing the noble metal for hydrogenation/dehydrogenation and molecular sieve for carbon–carbon bond rearrangement are known to be very effective in hydroisomerization of *n*-paraffins. Recently catalysts with high selectivity for the hydroisomerization of long-chain *n*-paraffin have been reported. These catalysts were composed of medium-pore silicoaluminophosphate (SAPO) molecular sieves [3–11], e.g., SAPO-11 (AEL), SAPO-31 (ATO) and SAPO-41 (AFO). Some reports [10, 12] revealed that the high activity and selectivity of these catalysts in isomerization were due to their unique combination of mild acidity and shape selectivity. Generally speaking, acid strength of SAPOs is weaker than that of zeolites. But catalysts based on ZSM-23 (MTT) and ZSM-22 (TON) with 10-membered channels also exhibited higher selectivity for isomerization than hydrocracking [13–17]. Many works only concentrate on one family of molecular sieves without consideration of another.

The study is aiming at examining at the effects of channel structure and acidity of molecular sieves on hydroisomerization of *n*-octane over the two families of molecular sieves. Comparison of the behavior of SAPOs to that of zeolites would provide an overall approach to accomplish the study. In addition to molecular sieves above mentioned, SAPO-5 (AFI), -34 (CHA) and ZSM-5 (MFI) which are representative of large-pore, small-pore, zigzag channel type of molecular sieves were investigated.

2. Experimental

2.1. Catalyst preparation

The molecular sieves used in this study were synthesized in our lab. The gel composition and synthesis conditions are presented in table 1. SAPO-5, SAPO-11, SAPO-31, SAPO-41 and SAPO-34 were synthesized with the following procedure according to Refs. [18–21]. Aluminum compound (pseudoboehmite or aluminum isopropoxide) was slowly added to the mixture of orthophosphoric acid and distilled water with vigorous stirring. Next fumed silica (or silica sol) and the template

*To whom correspondence should be addressed.
E-mail: guoxw@dlut.edu.cn; huyfdqlh@yahoo.com.cn.

Table 1
The gel composition and synthesis conditions of the molecular sieves

Molecular sieves	Al	P	Si	Template	Time[a] (h)	Temperature[b] (°C)
SAPO-5	$Al(OPr^i)_3$[c]	H_3PO_4[d]	Fume silica	Di-*n*-butylamine	24	170
SAPO-11	Boeh[e]	H_3PO_4	Fume silica	Di-*n*-propylamine	24	170
SAPO-31	Boeh	H_3PO_4	Fume silica	Di-*n*-propylamine	24	170
SAPO-41	Boeh	H_3PO_4	Tetraethyl-orthosilicate	Di-*n*-propylamine + ethanol	24	170
SAPO-34	Boeh	H_3PO_4	Silica sol[f]	morpholine	24	190
ZSM-22	$NaAlO_2$		Silica sol	Hexane-1,6-diamine	48	180
ZSM-23	$NaAlO_2$		Silica sol	pyrrolidine	48	180
ZSM-5	$NaAlO_2$		Silica sol	Tetrapropylammonium hydroxide	48	175

[a]Time of crystallization.
[b]Temperature of crystallization.
[c]Aluminium isopropoxide.
[d]Phosphoric acid, 85%.
[e]Pseudoboehmite.
[f]Silica sol, 30%.

were added in turn and the resulting mixture was stirred until it was homogeneous. The gel mixture was crystallized with no stirring under autogenous pressure in a 100 cm^3 stainless-steel autoclave lined with PTFE. Crystalline products were filtered, washed with deionized water and dried overnight at 100 °C, and then calcined at 500 °C under oxygen flow in order to remove the template completely.

During the synthesis of ZSM-5, ZSM-22 and ZSM-23, $NaA1O_2$ and silica sol were used as the starting materials [22–24]. An aluminate solution was made by completely dissolving $NaAlO_2$ and NaOH into distilled water. Template was added to the aluminate solution followed by silica sol. Na-form zeolites were converted into H-form zeolites by treated with 1 M NH_4NO_3 solution (three times,100 ml of solution per 1 g of zeolite) and calcined at 500 °C under oxygen flow.

The dry molecular sieve powder was impregnated with $Pt(NH_3)_4Cl_2$ to obtain a Pt loading of 0.5%, and calcined at 350 °C. The powder was shaped into tablets by compression, the tablets were crushed and then sieved to obtain catalyst pellets with diameter of 20–40 mesh.

2.2. Characterization

The chemical composition of solids (Al, Si and P) was determined by Bruker SRS 3400 XRF spectrometer. X-ray diffraction patterns were recorded on a Shimadzu 2000 diffractometer (40 kV, 30 mA) using Cu K radiation and an angle scanning speed of 2° min^{-1} between 2° and 50°. The crystal size and habit of these molecular sieves were obtained on a JEOL JSM-6360LA Scanning Electron Microscope (SEM). NH_3 temperature programmed desorption (NH_3-TAD) was performed in a flow system equipped with a TCD detector. 0.2 g of the sample was first flushed with He (40 ml min^{-1}) at 450 °C for 1 h, then cooled to 120 °C, and saturated with NH_3 until equilibrium was reached. The sample was heated in a linear rate 10 °C min^{-1} to 500 °C, and the signal of desorbed ammonia was recorded from 120 °C to 500 °C.

2.3. Catalytic test

The catalytic conversion of *n*-octane was carried out in a down flow fixed-bed stainless reactor. The reaction conditions were as following: pressure 1.0 MPa, *n*-octane WHSV 2.0, H_2/*n*-octane molar ratio 2. The catalyst was reduced *in situ* in a flow of H_2 at 410 °C for 1 h prior to the start of the reaction. Gas products were analyzed on-line by GC-8A gas chromatography equipped with sebaconitrile/PAW packed column, and liquid products by GC-8A gas chromatography equipped with an OV-101 capillary column.

3. Results and discussion

3.1. Synthesis of molecular sieves

In figure 1, the XRD data of the as-synthesized samples confirmed the structure types SAPO-5, SAPO-11, SAPO-31, SAPO-41, SAPO-34, ZSM-5, ZSM-22 and ZSM-23. The patterns, both in intensity and line position, were in very good correspondence with that in the literature. The high intensity of XRD lines and low background in the XRD patterns indicate high crystallinity of the samples. Practically no loss in crystallinity was observed when these materials were calcined in order to remove the organic templates. These results are in agreement with that of SEM, in which we can observe agglomerate of a great many of small crystals between 1 and 5 μm except for SAPO-34 with single crystals of 5–10 μm and a very low concentration of amorphous substance. The chemical composition and the structure characteristics [25] of the solid products are given in table 2.

In SAPOs cases, the silicon atoms can enter into the aluminophosphate framework via substitution of a

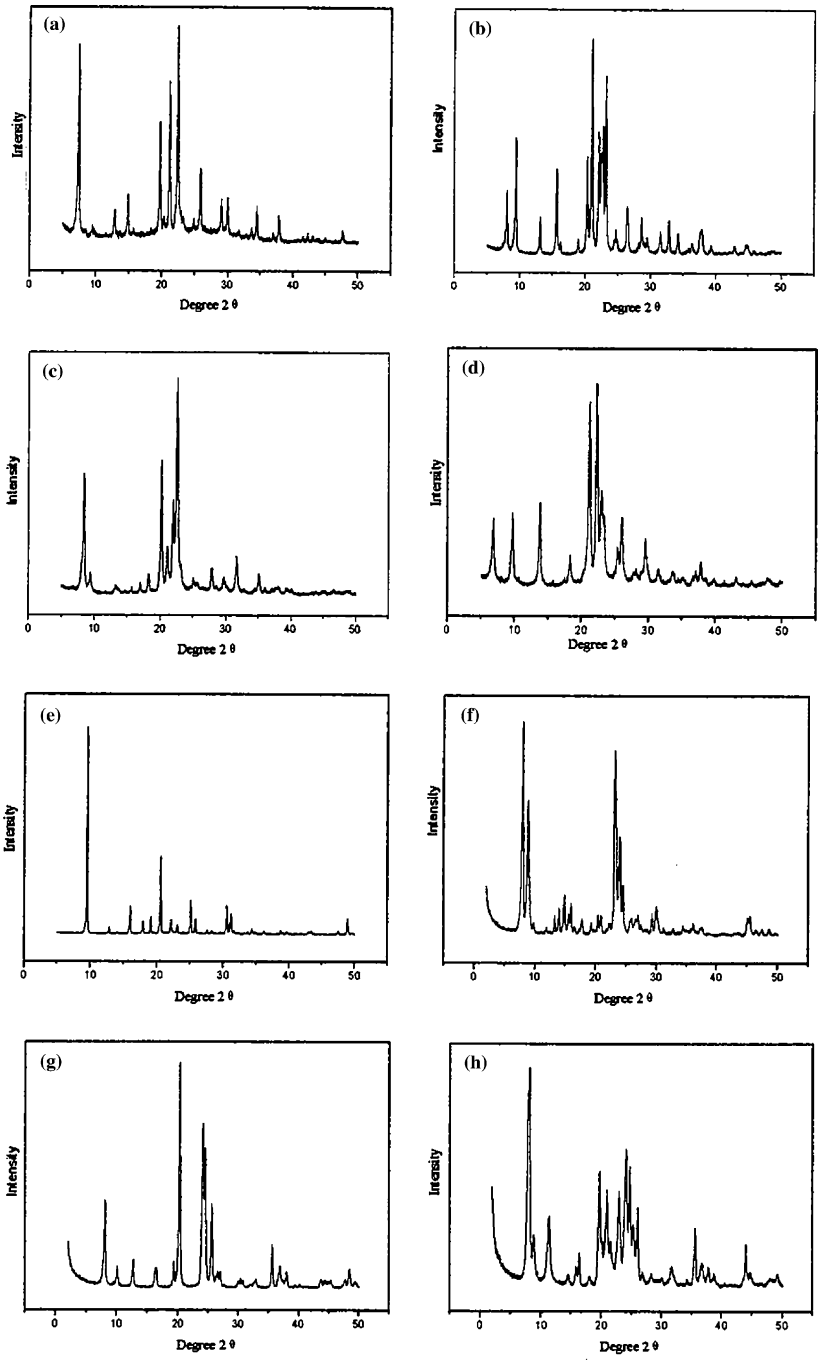

Figure 1. XRD patterns of SAPO and aluminosilicate samples: (a) SAPO-5; (b) SAPO-11; (c) SAPO-31; (d) SAPO-41; (e), SAPO-34; (f) ZSM-5; (g) ZSM-22; (h) ZSM-23.

single Si for a single P and two Si for one Al and one P [26,27]. From chemical composition, it can be concluded that the substitution of single Si for single P predominates in SAPO-5, −31, −41, −34 and the substitution of two Si for one Al and one P predominates in SAPO-11.

3.2. *Effect of pore size on hydroisomerization of n-octane*

The results of *n*-octane conversion over Pt/SAPO-5, −11, −31, −41 and −34 are presented in table 3, In the hydroconversion of *n*-octane, hydroisomerization and hydrocracking occur simultaneously and competitively. It is remarkable that Pt/SAPO-5 exhibits both the highest conversion activity and the highest cracking selectivity and Pt/SAPO-34 has the lowest conversion activity among the different Pt/SAPOs studied. Catalysts prepared with medium-pore SAPOs, i.e., Pt/SAPO-11, −31 and −41, show higher selectivity to hydroisomerization at higher conversion activity.

Isomerization of long chain *n*-paraffin on bifunctional catalysts can be explained by the existence of classical (alkyl-shifts isomerization) as well as non-classical

Table 2
Chemical composition and main characteristics of the molecular sieves

Molecular sieves	Structure type	D[a]	windows[b]	Channel dimensions (Å)	Al[c] (%)	Si[c] (%)	P[c] (%)
SAPO-5	AFI	1	12MR	7.3	48.0	9.0	43.0
SAPO-11	AEL	1	10MR	6.5 × 4.0	44.0	12.8	43.2
SAPO-31	ATO	1	12MR	5.4	52.0	4.0	44.0
SAPO-41	AFO	1	10MR	7.3 × 4.0	49.9	5.3	44.8
SAPO-34	CHA	3	8MR	3.8	50.0	15.0	35.0
ZSM-23	MTT	1	10MR	4.5 × 5.2	2.8	97.2	
ZSM-22	TON	1	10MR	4.6 × 5.7	3.3	96.7	
ZSM-5	MFI	3	10MR	5.5 × 5.1 + 5.6 × 5.3	3.8	96.2	

[a]Dimensionality of the porous structure.
[b]MR, member ring of oxygen atoms.
[c]Expressed as $(Si_xAl_yP_z)O_2$.

Table 3
Conversion of n-octane over Pt/SAPO-5, −11, −31, −41 and −34

Catalysts	Pt/SAPO-5	Pt/SAPO-11	Pt/SAPO-31	Pt/SAPO-41	Pt/SAPO-34
Products (wt%)					
C^0_1–C^0_3	10.91	1.54	4.98	4.86	0.51
iC^0_4	20.00	2.11	3.68	3.42	0.07
nC^0_4	10.90	2.33	4.72	4.12	0.19
iC^0_5	16.47	0.91	1.94	1.88	0.07
$nC5^0$	2.67	0.71	2.27	2.23	0.23
$C6^0$–$C7^0$	2.48	0.17	1.74	1.64	0.53
DMC^{0a}_6	6.87	17.62	22.47	15.53	0
MC^{0b}_7	19.93	56.85	47.25	52.93	2.73
n-C^0_8	8.45	16.76	10.50	12.09	95.49
Other products	1.34	1.01	0.45	1.28	0.39
Conversion (wt%)					
n-C^0_8	91.55	83.24	89.50	87.91	4.51
Selectivity (%)					
Cracking products[c]	69.26	9.32	21.61	20.66	35.48
DMC^0_6	7.50	16.77	25.11	17.67	0
MC^0_7	21.77	68.30	52.79	60.21	60.53

Reaction Temperature: 340 °C, TOS (time on stream): 12–24 h.
[a]DMC^0_6: 6 isomers of dimethlyC^0_6.
[b]MC^0_7: 3 isomers of methyl C^0_7.
[c]Cracking products: C^0_1–C^0_7.

mechanism (protonated cyclopropane isomerization) at the catalyst surface [28,29]. The exact nature of the mechanism is not important in the paper. We are interested in the analysis of the cracked products for exploring the reason of hydrocracking. Martens *et al.* [30] classified four types of β carbon–carbon bond scission (Scheme 1) about mechanistic aspects of hydrocracking. The scheme indicates that the high isomer yields found in the cracked products is the result of primary cracking of multibranched intermediates.

In table 3, the ratio of iC^0_4/nC^0_4 and iC^0_5/nC^0_5 over Pt/SAPO-5 is the highest, i.e., 1.83 and 6.17. The secondary isomerization of nC^0_4 and nC^0_5 is excluded owing to constraint of thermodynamic equilibrium. From thermodynamic equilibrium views, it is impossible to gain such high ratio in the temperature of 340 °C [31]. So major hydrocracking over Pt/SAPO-5 is ascribed to cracking of tribranched and dibranched alkylcarbenium ions, especially tribranched alkylcarbenium ions. In Scheme 1, the relative rates increase drastically from A scission mode to C scission mode. Occurrence of these bulkier ions is in agreement with large pore size of SAPO-5. Among different SAPOs studied, SAPO-5 has the largest pore, 12-membered ring of 0.73 nm, which provides sufficient space for the formation of cracking precursors and leads to the lowest selectivity to isomerization. By comparison with SAPO-5, 8-membered ring of 0.38 nm in SAPO-34 is smaller than the kinetic diameter of branched C^0_8 isomers, most of the acid sites do not catalyze isomerization of *n*-octane. A very small conversion (about 5%) over Pt/SAPO-34 can be explained by the function of external acid sites.

In the channels of medium-pore SAPOs, formation of multibranched alkylcarbenium ions that are susceptible to cracking is suppressed in the presence of steric or geometric constraints. So the isomerization selectivity can be enhanced. Although SAPO-31(ATO) has 12-membered ring channels in the structure, the

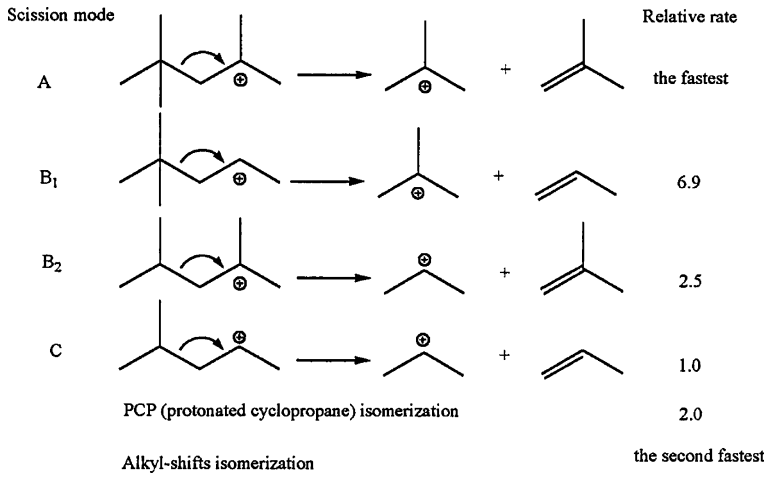

Scheme 1. β-scission modes acting on secondary and tertiary carbonations.

nearly circular opening with an effective diameter of 0.54 nm brings it under the medium-pore category [32]. A.K. Sinha *et al.* [4] and P. Meriaudeau *et al.* [10,11] studied *n*-octane isomerization over Pt-loaded medium-pore SAPOs, i.e., Pt/SAPO-11, -31 and -41. They found out the difference in isomerization selectivity of these SAPOs. For comparison, variation of the isomerization selectivity with the conversion was done by tentatively changing the reaction temperature. In figure 2, medium-pore SAPOs exhibit good selectivity to isomerization (>90%) until high conversion (80%) and negligible difference in the curves of Pt-loaded medium-pore SAPOs is obtained. So the difference in isomerization selectivity among these catalysts shown in table 3 should be understood as the result of difference in their conversion other than the difference in their pore dimensions.

3.3. *Effect of the number of acid sites over medium-pore SAPOs on hydroisomerization of n-octane*

M. Hochtl *et al.* [5] and Meriaudeau *et al.* [10] once reported that the content of Pt (0.5%) and the Pt dispersion obtained by the impregnation were sufficient to provide the dehydrogenation activity sites to balance the acid sites of catalysts. Hence, in this paper, we think that the *n*-octane hydroconversion activity of Pt/SAPOs is essentially governed by characteristics of molecular sieves. The TPD profiles of NH_3-desorption on calcined SAPOs are showed in figure 3. SAPO-5, -11, -31 and -41 only have the NH_3-desorption peak of low temperature. Area of the NH_3-desorption peak indicates the number of acid sites increases in the order of SAPO-11 < SAPO-41 < SAPO-31 < SAPO-5. Correlated with the catalytic performances in table 3, it can be seen that the hydroconversion activity of catalysts increases with the

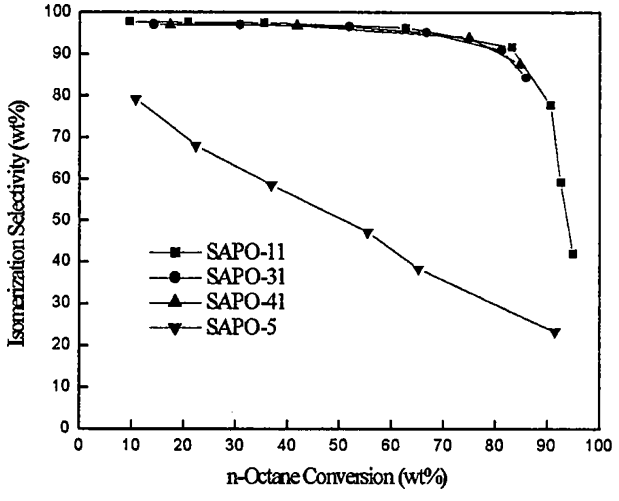

Figure 2. Isomerization selectivity over Pt/SAPO-11, -31, -41 and -5 as a function of the conversion of *n*-octane. The range of reaction temperature over Pt/SAPO-5, -11, -31 and -41 is 285–340 °C, 295–340 °C, 295–390 °C and 295–340 °C respectively.

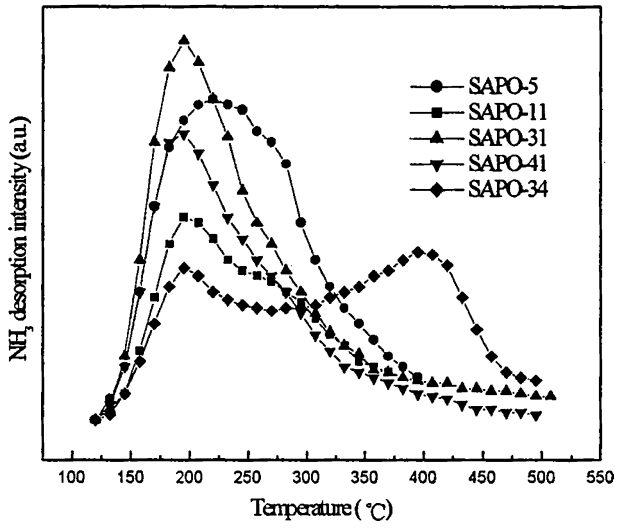

Figure 3. NH_3-TPD profiles of the SAPOs.

number of the weak acid sites of the SAPOs. In table 3, the conversion of *n*-octane over Pt/SAPO-11, -41, -31 and -5 is 83.24%, 87.91%, 89.50% and 91.55% respectively. For medium-pore SAPOs, a minor difference in high conversion (>80%) can lead to major difference in distribution of products.

Distribution of products in *n*-octane isomerization over Pt/SAPO-11 as a function of the conversion is given in figure 4. It is clear that DMC^0_6 becomes increasing important with increase of the conversion and the maximum yield of DMC^0_6 is observed at the conversion of 92%. Figure 4 contains enough evidence for the general statement that formation of DMC^0_6 over Pt/SAPO-11 is accelerated at high conversion (>80%), inducing consecutive transformation into cracking products. So distribution of products changes remarkably when the conversion goes through 80%. These results also account for distribution of products of two other medium-pore SAPOs in table 3.

3.4. *Effect of acid strength on hydroisomerization of n-octane*

The TPD profiles of NH_3-desorption on ZSM-5, -22 and -23 (figure 5) show that in addition to the NH_3-desorption peak of low temperature which is similar with medium-pore SAPOs, ZSM-22 and -23 have the high temperature NH_3-desorption peak around 430 °C. This indicates that ZSM-22 and -23 have not only weak acid sites but also strong acid sites.

Conversion of *n*-octane at various temperatures over Pt/ZSM-5, -22 and -23 is listed in table 4. Upon comparison of table 3 and table 4, it is showed that the reaction temperature of Pt/ZSM-22 and -23 for higher yield of isomers is lower than that of Pt/SAPOs. The difference of the reaction temperature can be understood as the result of different acid strength. So we can conclude that strong acid sites are helpful to decrease active energy of the rate-limiting step and increase the conversion activity. Park *et al.* [12] attributed higher hydrocracking selectivity to strong acid sites of molecular sieves. But in the curves of isomerization selectivity changing with the conversion (figure 6), Pt/ZSM-22 and -23 still exhibit good selectivity to isomerization under high conversion and are very similar to Pt-loaded medium-pore SAPOs in figure 2. Strong acid sites of medium-pore ZSM-22 and -23 have no unfavorable effect on high selectivity to isomerization.

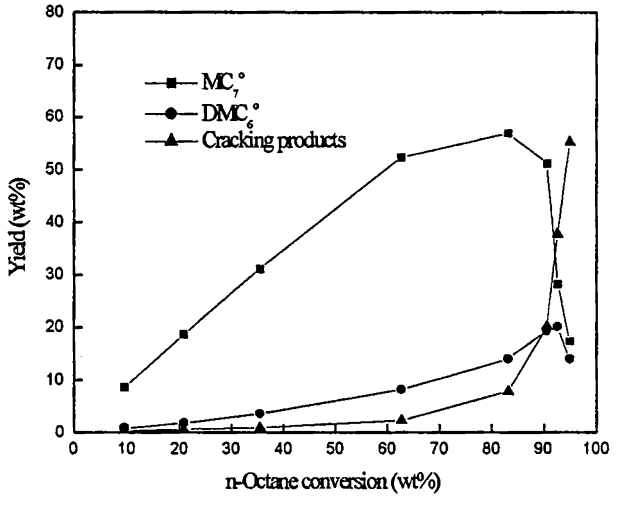

Figure 4. Distribution of major products in *n*-octane isomerization over Pt/SAPO-11 as a function of the conversion of *n*-octane. The reaction conditions are the same as that in figure 2.

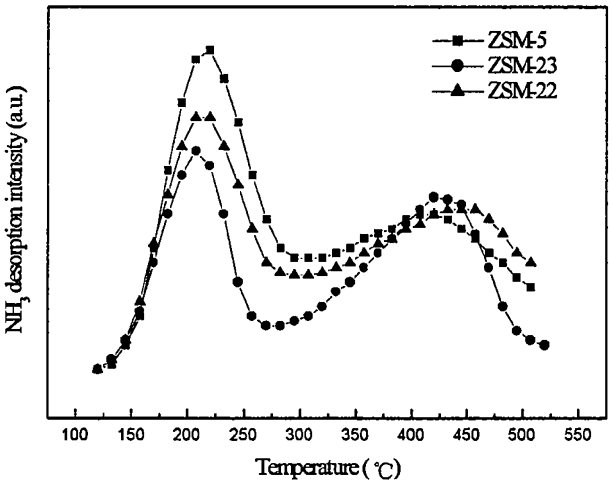

Figure 5. NH_3-TPD profiles of the ZSM-5, -22 and -23.

3.5. *Effect of shape of medium-pore channel on hydroisomerization of n-octane*

In the study, these medium-pore molecular sieves only contain a straight channel system except for

Table 4
Conversion of *n*-octane at various temperatures over Pt/ZSM-5, -22 and -23

Catalysts	Pt/ZSM-5	Pt/ZSM-22		Pt/ZSM-23	
Temperature (°C)	236	290	340	290	340
Products (wt%)					
C^0_1–C^0_3	7.58	3.72	16.76	1.83	6.48
iC^0_4	8.62	1.62	11.45	1.46	13.35
nC^0_4	10.47	3.90	25.25	1.80	20.25
iC^0_5	7.15	2.14	23.69	0.46	9.90
nC^0_5	13.25	2.19	12.86	0.61	6.01
C^0_6–C^0_7	10.59	0.98	1.72	0.38	1.46
DMC^0_6	1.82	12.68	3.15	2.99	12.66
MC^0_7	5.65	59.26	1.89	60.77	19.08
n-C^0_8	31.27	13.50	1.24	28.94	8.05
Other products	3.60	1.61	1.99	0.74	2.75
Conversion (wt%)					
n-C^0_8	68.73	86.50	98.76	71.06	91.05
Selectivity (%)					
Cracking products	83.89	16.75	92.88	9.22	63.11
DMC^0_6	2.65	14.66	3.19	4.92	13.90
M C^0_7	8.22	68.51	1.91	85.52	20.96

TOS (time on stream): 12–24 h.

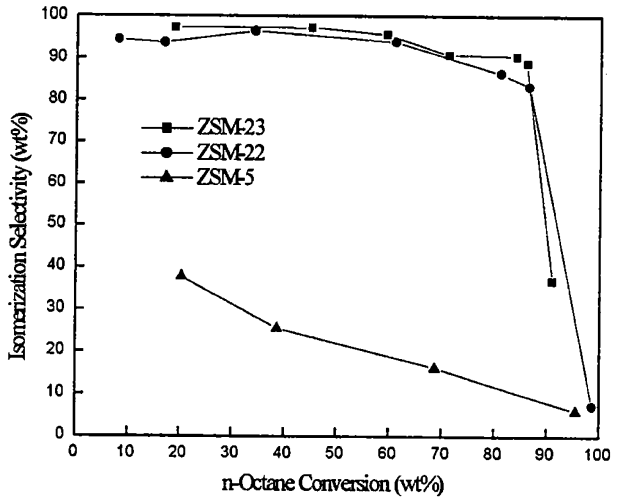

Figure 6. Isomerization selectivity over Pt/ZSM-23, -22 and -5 as a function of the conversion of *n*-octane. The range of reaction temperature over Pt/ZSM-5, -22 and -23 is 203–246 °C, 215–340 °C and 225–340 °C respectively.

ZSM-5. The ZSM-5 contains not only a straight 10-ring channel system but also a zigzag 10-ring channel system. So the effect of shape of medium-pore channel can be examined with ZSM-5. Figure 6 shows that hydrocracking becomes predominant over Pt/ZSM-5 even at low conversion (less than 20%).

Upon comparison of figures 2 and 6, the hydrocracking behavior over Pt/ZSM-5 is different from that of Pt/SAPO-5. Hydroisomerization of *n*-octane over Pt/SAPO-5 is the predominant reaction at low conversion (less than 20%), while hydrocracking of *n*-octane over Pt/ZSM-5 is serious even at low conversion (less than 20%). In table 4, $iC^0{}_4/nC^0{}_4$ and $iC^0{}_5/nC^0{}_5$ over Pt/ZSM-5 are 0.82 and 0.54 respectively, which are much lower than that of Pt/SAPO-5. The differences reflect that cracking, over Pt/ZSM-5 is principally through C scission mode while cracking over Pt/SAPO-5 is principally through A, B_1 and B_2 scission mode. The difference is not attributed to strong acid sites of ZSM-5, because C mode scission over Pt/ZSM-22 and −23 with similar acid strength (shown in figure 5) is not serious even at high conversion. This can be related to a slower migration of the intermediates within the zigzag 10-ring channel and longer life-time of the intermediates [28], leading to an enhanced hydrocracking selectivity. So the enhanced hydrocracking selectivity over Pt/ZSM-5 is due to the longer lifetime of the intermediates other than the formation of multibranched alkylcarbenium ions.

4. Conclusions

The selectivity to isomerization in hydroisomerization of *n*-octane is highly influenced by the pore structure in molecular sieves. Bulkier shape and longer life-time of carbenium ions are in favor of cracking of the intermediates. The absence of steric or geometric constraints in SAPO-5 and a slower migration in the zigzag channel of ZSM-5 are responsible for low isomerization selectivity of corresponding catalysts. Preferential isomerization has been observed on monodimensional medium-pore molecular sieves regardless of acid strength, such as SAPO-11, -31, -41, ZSM-22 and -23. The conversion activity of *n*-octane is dependent on the acidity of molecular sieves, both more acid sites and stronger acid sites increase the conversion of *n*-octane.

References

[1] K.W. Smith, W.C. Starr and N.Y. Chen, Oil. Gas. J., May 26 (1980) 75.
[2] S J. Miller, Zeolites and Related Microporous Materials: State of the Art 1994, Stud. Surf. Sci. Catal., Vol. 84, Elsevier, Amsterdam, 1994, p. 2319.
[3] S.J. Miller, U. S. Patent 5,246,566 (1993).
[4] A.K. Sinha and S. Sivasanker, Catal. Today 49 (1999) 293.
[5] M. Hochtl, A. Jentys and H. Vinek, Catal. Today 65 (2001) 171.
[6] J.M. Campelo, F. Lafont and J.M. Marinas, Appl. Catal. A 170 (1998) 139.
[7] F. Zhang, C.H. Geng, Z.X. Gao and J.L. Zhou, Chin. J. Catal. 25 (2004) 431.
[8] Y.M. Liu, F.M. Zhang, X.T. Shu and M.Y. He, Chin. J. Catal. 24 (2003) 781.
[9] I. Eswaqramoothi and N. Lingappan, J. Mol. Catal. A 218 (2004) 229.
[10] P. Meriaudeau, V.A. Tuan, V.T. Nghiem, S.Y. Lai, L.N. Hung and C. Naccache, J. Catal. 169 (1997) 55.
[11] P. Meriaudeau, V.A. Tuan, G. Sapaly, V.T. Nghiem, S.Y. Lai and C. Naccache, Catal. Today 49 (1999) 285.
[12] K.C. Park and S.-K. Ihm, Appl. Catal. A 203 (2000) 201.
[13] P. Raybaud, A. Patrigeon and H. Toulhoat, J. Catal. 198 (2001) 98.
[14] T.L. Maesen, M. Schenk, T.J.H. Vlugt, J.P. Jonge and B. Smit, J. Catal. 188 (1999) 403.
[15] M.C. Claude, G. Vanbutsele and J.A. Martens, J. Catal. 203 (2001) 213.
[16] M.C. Claude and J.A. Martens, J. Catal. 190 (2000) 39.
[17] P. Raybaud, A. Patrigeon and H. Toulhoat, J. Catal. 197 (2001) 98.
[18] B.M. Lok, C.A. Messing, R.L. Patton, R.T. Gajek, T.R. Cannan and E.M. Flanigen, U. S. Patent 4,440,871 (1984).
[19] S.j. Miller, U. S. Patent 5,158,665 (1992).
[20] S.j. Miller, U. S. Patent 5,230,881 (1993).
[21] Y.F. Hu, X.S. Wang, X.W. Guo, P. Xu and S.L. Li, Chin. J. Catal. 25 (2004) 87.
[22] B.M. Lowe and A. Araya, U. S. Patent 4,900,528 (1990)..
[23] S.I. Zones, J.N. Ziemer, D.S. Santilli, R.A. Innes, S. Rafael and D.L. Holtermann, U. S. Patent 5,300,210 (1994)..
[24] X.Q. Wang, X.S. Wang and X.W. Guo, CN Patent 1,240,193 (2000).
[25] C. Baerlocher, W.M. Meier and D.H. Olson, *Atlas of Zeolite Framework Types* (Elsevier, Amsterdam, 2001).
[26] C.M. Zicovich-wilson, P. Viruela and A. Corma, J. Phys. Chem. 99 (1995) 13224.
[27] V.B. Kazanski and I.N. Senchenya, J. Catal. 119 (1989) 108.
[28] J.A. Martens and P.A. Jacobs, Zeolites 6 (1986) 334.
[29] J. Weitkamp and S. Ernst, Catal. Today 19 (1994) 107.
[30] J.A. Maetens, P.A. Jacobs and J. Weitkamp, J. Appl. Catal. 20 (1986) 283.
[31] I.E. Maxwell, Catal. Today 2 (1987) 385.
[32] J. Bennett and R.M. Kirchner, Zeolites 12 (1992) 338.